Rev. Roum. Sci. Techn.– Électrotechn. et Énerg.
Vol. **68**, *3*, pp. 283–288, Bucarest, 2023

ANALYZING A THREE HUNDRED TEETH BI-PHASE HYBRID STEPPER MOTOR WITH DIFFERENT NUMBERS OF POLE PAIRS

TEODOR IONUȚ ICHIM[1], OVIDIU CRAIU[2], LIVIU CRISTIAN POPESCU[3]

Keywords: Hybrid stepper motor; Finite Element Method (FEM); Holding torque; Detent torque.

The paper presents numerical models of a bi-phase, 0.3° full step hybrid stepper motor (HSM), with 16, 24, 32, 40, and, respectively, 48 poles in the stator. For the motor to move with a constant step angle, the stator and the rotor teeth must be shifted against each other with an angle of zero, 90, 180, and 270 electric degrees for each four consecutive stator poles. Due to this, bi-phase steppers with the number of poles in the stator different than eight are hardly seen. Therefore, to allow the construction of HSMs with different numbers of poles, some of the stator poles must be shifted from their symmetrical position. The five topologies' HSM detent and holding torque characteristics and their geometrical and constructive differences are presented. The Finite Element Method (FEM) based models are developed using the professional software COMSOL Multiphysics.

1. INTRODUCTION

The HSM are synchronous motors used for precise positioning [1]. In many applications, they operate as actuators where resolution, sensitivity, and accuracy are important factors. Also, the HSM has a high torque density, an advantage where miniaturization is important. The most common HSMs are bi-phase and have a full step of 1° or 1.8° per step. The moving step can be significantly reduced by controlling the phase currents to even 0.036° [2]. Due to its simplicity and robustness, open-loop drives with full step movement are preferred in most space applications using stepper motors.

The HSM presented in this paper is special because it has a full step of 0.3 mechanical degrees, one of the smallest known. Achieving such a small step means a construction with 300 teeth in the rotor, which requires a very refined production. To make things even more challenging, the HSM are machines with very small air gaps of fractions of millimeters [3].

Modeling these machines is, therefore, difficult. As the magnetic field produced by the stator armature coil is transversal and the magnetic field produced by the rotor magnet is axial, the only way to study these motors by numerical models is using 3D numerical models. Analytical models are limited in producing accurate results [1, 4–6], as well as the hybrid analytical-numerical models or the hybrid 2D-3D numerical models, despite their reduced computational costs [4]. Due to their complexity, high computational effort, and increased computer memory requirement, the 3D FEM-based studies of the HSMs remain scars [7–10].

Another specific of the bi-phase HSMs is that they must have a multiple of four poles, each of the phases having an even number of poles in the stator. The stator teeth of one pole must be aligned with the rotor teeth beneath, and then, for the subsequent poles, the teeth are shifted by an additional quarter of the tooth pitch, which is 90 electrical degrees. The two rotor side crowns embrace the permanent magnet, which is axially magnetized, and have their teeth shifted against each other with half of a tooth pitch 180 electrical degrees. This alignment between the stator and rotor teeth cannot be achieved for any random combination of stator poles (which must be multiple of four) and rotor teeth if the poles are placed symmetrically around the stator yoke. To obtain the required stator-rotor teeth alignment, the authors propose shifting some of the stator poles from their symmetry axis with a very small and well-defined angle that does not modify the slot area and the room available for the winding noticeably. Some of the HSM topologies, however, do not require a pole shift, the teeth aligning in the right position for the poles placed symmetrically around the stator.

2. NUMERICAL MODELS

Five different topologies of the two-phase HSMs with 16, 24, 32, 40, and, respectively 48 stator poles were analyzed using 3D FEM models developed in COMSOL Multiphysics. To make possible a relevant comparison between these topologies, all HSM models had the same geometrical envelope defined by an external diameter D_{ext} = 157 mm, an inner rotor diameter larger than 125 mm, and an axial length of a maximum of 31 mm, including the end windings. At the same time, the airgap length was kept at 0.25 mm for all motors, the same $SmCo_{32}$ permanent magnet was used, as well as the same current density J = 1.5 A/mm^2 in the armature windings at a constant slot fill factor k_f = 0.33 (copper total area by slot area). Moreover, given that the ratio between the slot width and the tooth pitch influences the shape of the HSM holding torque and the detent torque characteristics [9, 11], this ratio was kept k_{sl} = 0.56 for all models. All HSMs have 300 teeth in the rotor, and both stator and rotor teeth are 0.6 mm in height.

Computing consecutive magnetic stationary field problems simulated the HSM rotor movement, one for each motion step. The Rotating Machinery Magnetic COMSOL module simulated the movement without rebuilding the mesh by sewing the stator and the rotor mesh through an airgap cylindrical surface to save computational time. This allowed us to compute the next movement step using the previous solution. The rotor was moved in small steps over 0.6 mechanical degrees, one-half of the electric period, while the current density **J** was kept constant in one phase and zero in the other. The end windings' influence on the motor torque was neglected.

The COMSOL *Rotating machinery, magnetic* module uses a combined formulation based on the magnetic vector potential vector **A** in the areas with current sources and the magnetic scalar potential V_m in the areas without current sources. The well-known governing equations are:

$$\Delta \mathbf{A} = -\mu \mathbf{J} \tag{1}$$

for the magnetic vector potential, and:

$$\nabla \cdot \left(\mu \nabla V_m \right) = \nabla \cdot \mathbf{B}_r \tag{2}$$

[1]University "Politehnica" of Bucharest, Splaiul Independenței 313, Bucharest, Romania. E-mails: ichim_teodor@yahoo.com, ocraiu@yahoo.com, liviu_p@yahoo.com

DOI: 10.59277/RRST-EE.2023.68.3.6

for the areas defined by the scalar potential. The motor permanent magnet was modeled considering a linear demagnetization characteristic defined by the remanent induction $\mathbf{B}_r$ and its equivalent magnetic permeability μ.

The vector potential **A** and the scalar potential V_m domains are connected using an implicit *Mixed Formulation Boundary* condition. According to COMSOL documentation, this ensures a "continuity condition between the magnetic scalar potential on one side of the boundary and the magnetic vector potential on the other side," [12, p.330]. This is achieved by applying the continuity of the normal component of the magnetic field density and the tangential component of the magnetic field intensity on the separation surface:

$$B_{n\mathbf{A}} = B_{nVm}, H_{t\mathbf{A}} = H_{tVm} \tag{3}$$

According to COMSOL tutorials, the best choice is to have the Mixed Formulation Boundary at the level of the motor airgap. However, the separation of the **A** and V_m domains can be anywhere if the V_m domains do not contain any current source and they do not fully encircle an **A** domain containing a current source. A more in-depth analysis of how the two types of domains can be chosen is presented in [13].

Therefore, to reduce the computation time of the current model, a cylindrical surface was placed at the level of the stator pole shoes, and the scalar potential zone was extended up to this boundary, the blue area in Fig. 1.

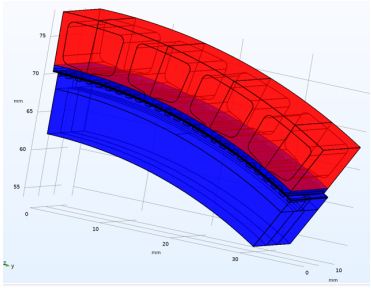

Fig. 1 – Magnetic vector potential **A** and scalar potential V_m domains.

In Fig.1 it is shown the computational domain that is 1/24th of the motor with 48 poles and two-stack rotor construction (1/12th of the circular domain representing one period and one-half of the axial direction representing one of the two rotor stacks).

The electromagnetic torque was computed using Arkkio's relation [14], a more accurate variant of the Maxwellian tensor that is used by default in COMSOL [12]:

$$T = \frac{1}{\mu_0 (r_e - r_e)} \int_{vol} r B_r B_\phi \, \mathrm{d}v \tag{4}$$

with *vol* the airgap volume comprised between the inner radius r_i and outer radius r_e, B_r and B_φ being the radial and tangential magnetic flux densities, respectively.

2.1 SIXTEEN-POLE HSM

Due to the motor's large slots and its thick end windings, the stator lamination stack was reduced to 14 mm to fit into the axial length of 31mm, and the motor was built as a "single stack" motor, Fig 2.

As the HSM has 16 poles, it was modeled 1/4th of the geometry using periodicity conditions on the side boundaries and continuity conditions on the sliding surface in the airgap, Fig. 3.a). A detail of the mesh discretization in the pole area is shown in Fig 3. b).

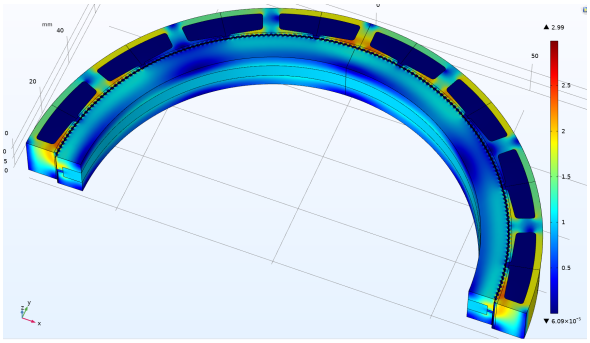

Fig. 2 – Half of the 16 poles HSM: magnetic flux density distribution.

To ensure the mesh resolution required for computing a very low torque like the detent torque, the mesh discretization used for modeling the load operation, Fig. 3.c) was refined at the airgap level, Fig. 3.d).

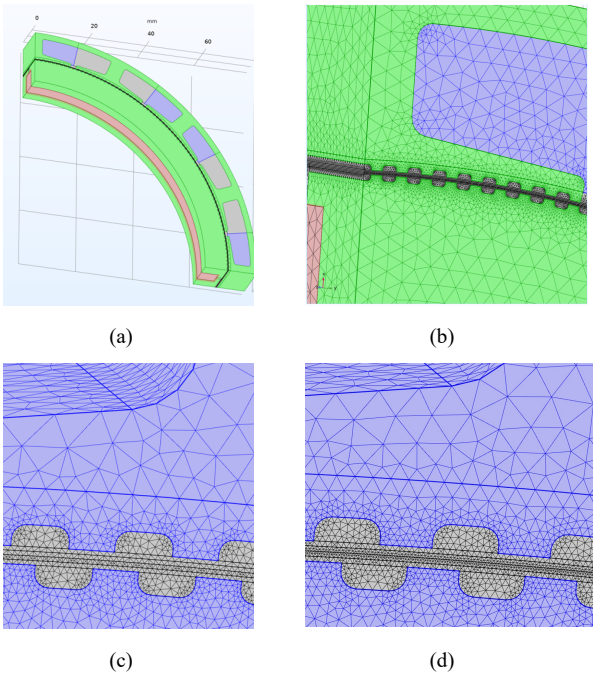

(a) (b)

(c) (d)

Fig. 3 – a) Computation domain (with iron, permanent magnet, and active windings marked in different colors), b) discretization mesh at shoe pole level, c) airgap mesh for load operation model, d) airgap mesh for no-load operation model.

The stator and the rotor teeth are aligned accordingly, without the need to adjust the motor geometry.

2.2 TWENTY-FOUR-POLE HSM

The motor is made as a double-stack motor, consisting of two "sandwiches" of two rotor crowns embedding each one a permanent magnet, Fig. 4.

The 24-pole HSM model consists of 1/6th of the circular geometry, which was subsequently divided in half along the axial length, due to its physical symmetry. The total rotor length is 18 mm, which allows sufficient space for the end windings without exceeding the motor's maximum length of 31mm. In Fig. 5. is shown the computational domain, with periodic conditions imposed on the side boundaries.

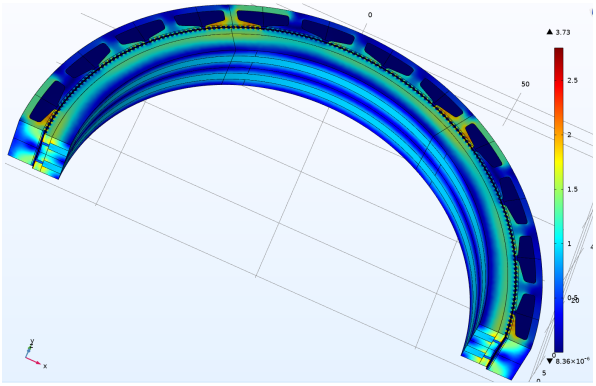

Fig. 4 – Half of the HSM with 24 poles and double stack construction: magnetic flux density distribution.

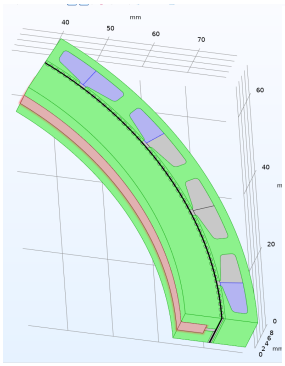

Fig. 5 – Computational domain and the different materials used in different colors, for the 24-pole HSM.

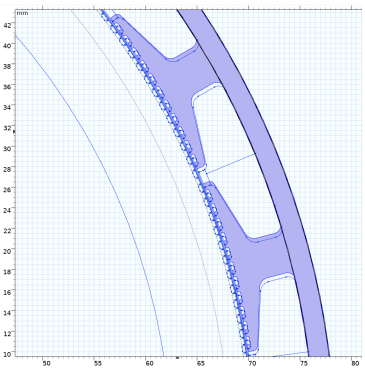

Fig. 6 – The pole must be shifted from its current position (in grey) to a new position (blue line) with 0.3°.

Different from the previous model where stator poles of the two phases alternate one after the other, this HSM has every two consecutive poles part of the same phase. That is not a problem if the stator and rotor teeth are properly aligned, as previously explained. To achieve that, two poles out of every four poles were slightly shifted from their symmetry position.

Let us define θ_{sp} the angle of the stator first tooth edge placed on the p^{th} stator pole, and θ_{rk} the angle of the rotor k^{th} tooth edge measured from a reference axis which is chosen so that $\theta_{s1} = \theta_{r1} = 0$ (i.e., the first tooth edge on the first stator pole is aligned with the reference axis and with the first rotor tooth edge). The maximum number of teeth that can be placed on the stator pole n_{st} is (a reduced number of teeth is possible making wider the space between consecutive poles):

$$n_{st} = \mathrm{INT}\left(n_{rot} / 2p\right) = 12$$

where the number of rotor teeth is $n_{rot} = 300$ and the number of stator poles is $2p = 24$. Choosing the maximum number of teeth per stator pole ensures the highest magnetic coupling between the motor's armatures, and thus the maximum torque density per volume. With the above-mentioned notations, it results:

$$\begin{cases} \theta_{12} = 360° / 2p = 360° / 24 = 15°, \ldots \\ \theta_{r13} = 360° / n_{rot} \times (n_{st} + 1) = 360° / 300 \times 13 = 15.6°, \ldots \end{cases}$$

Based on the above example the data in *Table 1.* below was computed. The phase shift between the first tooth of each pole and its corresponding tooth underneath placed in the rotor is given by $[(\theta_{sp} - \theta_{rk}) \bmod 1.2]$, with 1.2 being the rotor tooth pitch expressed in mechanical degree. As in four poles the stator and rotor teeth must be shifted with 0°, 0.3°, 0.6°, and 0.9° respectively (which means 0, 90, 180, and 270 electric degrees corresponding to a rotor tooth pitch of 1.2°), pole number 2 and 3 must be shifted with 0.3° to ensure the correct stator teeth position against the rotor teeth, Fig. 6.

Table 1

The shifting angle for each pole to ensure teeth alignment.

pole number rotor tooth number	$p = 1$ $k = 13$	$p = 2$ $k = 13$	$p = 3$ $k = 13$	$p = 4$ $k = 13$	$p = 5$ $k = 13$
θ_{sp}	0°	15°	30°	45°	60°
θ_{rk}	0°	15.6°	31.2°	46.8°	62.4°
$(\theta_{sp} - \theta_{rk}) \bmod 1.2$	0°	0.6°	0°	0.6°	0°
pole shift angle	0°	0.3°	0.3°	0°	0°

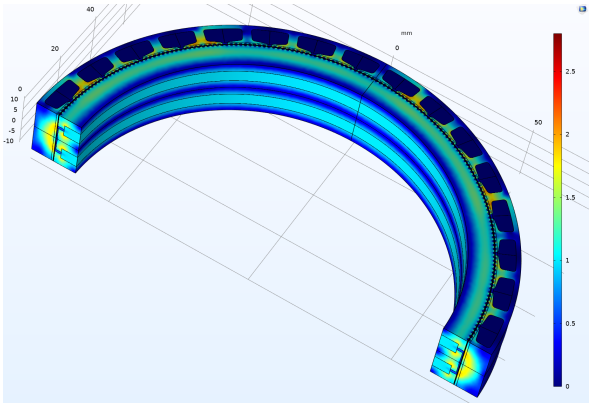

Fig. 7 – Half of the HSM with 32 poles and double stack construction: magnetic flux density distribution.

2.3 THIRTY-TWO-POLE HSM

The 32-pole HSM has even more compact coils and smaller end windings, allowing the extension of the stator and rotor iron to l_{axial} = 22mm out of a total of 31 mm. That allowed the construction of a double-stack rotor, Fig. 9.

The stator and rotor teeth are aligned in their position without the need to shift any of the stator poles from their symmetrical position.

Due to its physical symmetry, 1/4th of the circular geometry and one-half of the axial geometry (i.e., one of the two rotor stacks) was considered, which allowed a reduction of computation time and used memory. The computational domain, as well as the material used (light green is the iron core, brown is the permanent magnet and blue is the active winding), are shown in Fig. 8.

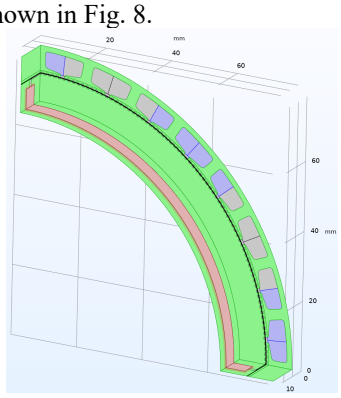

Fig. 8 – Computational domain and the different materials used in different colors, for the 32-pole HSM.

2.4 FORTY-POLE HSM

The 40-pole HSM was modeled as a double-stack motor with an axial rotor length of 22mm. Half of the geometry and

magnetic field density distribution is shown in Fig. 9.

Using motor physical symmetry, only 1/12th of the circular geometry and half of the axial length (one of the two stacks) were modeled. The same colors represented the materials: light green for the iron core, brown for the permanent magnet, and blue for the active coils in blue, Fig. 10.

To align the stator teeth with the rotor teeth under the different poles with 0, 90, 180, and 270 electrical degrees, a similar procedure used for the 24-pole HSM model was applied. Two poles in every four were shifted with -0.3° from their symmetry axis, placing the stator teeth in the right position with the rotor teeth without a noticeable modification of the slot area, Fig. 11.

Fig. 9 – Half of the HSM with 40 poles and double stack construction: magnetic flux density distribution.

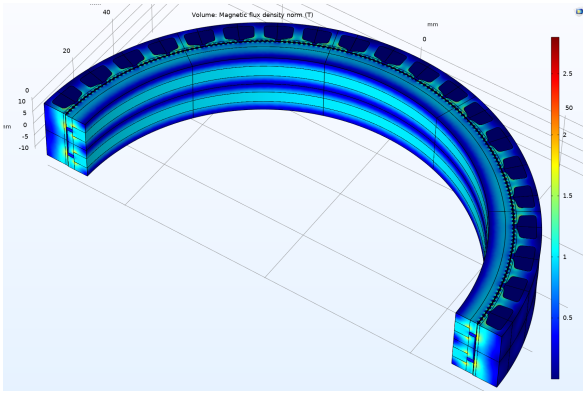

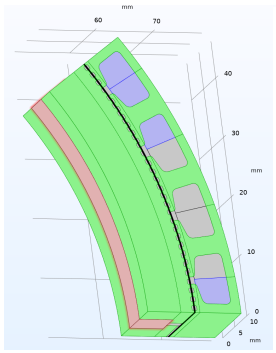

Fig.10 – Computational domain and the different materials used in different colors, for the 40-pole HSM.

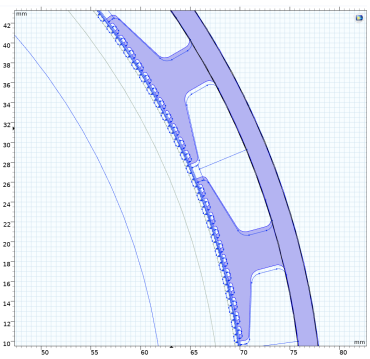

Fig. 11 – pole must be shifted from its current position (in grey) to a new position (blue line) with -0.3°.

2.5 FORTY-EIGHT-POLE HSM

The 48-pole HSM was modeled also as a double-stack motor with an axial rotor length of 24 mm. Half of the motor geometry and magnetic flux distribution are shown in Fig. 12. The motor is a double-stack motor.

Based on physical symmetry, the computational domain was reduced to 1/12th of the circular domain and half of the axial length (i.e., one of the two rotor stacks). The materials and the active coils (in blue) are shown in Fig. 15. The stator and rotor teeth aligned without the need to shift any of the stator poles from their initial symmetrical position.

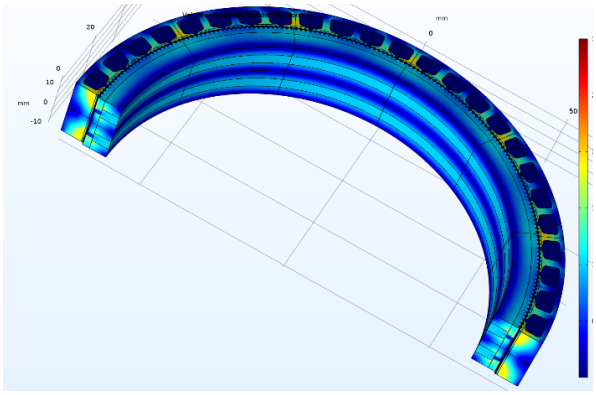

Fig. 12 – Half of the HSM with 48 poles and double stack construction: magnetic flux density distribution.

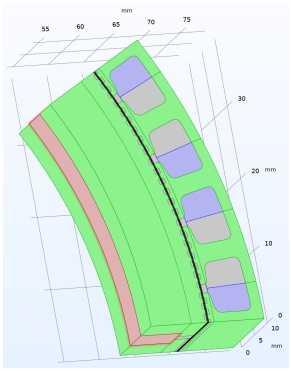

Fig.13 – Computational domain and the different materials used are plotted in different colors, for the 48-pole HSM.

3. RESULTS

The two main characteristics of the HSM are the holding torque, which defines the torque variation against the rotor position when the current is maintained constant in one phase, and the detent torque characteristic, which defines the cogging torque variation with the rotor position [15].

The purpose of the current HSM design was to identify the stepper motor with the highest holding torque and the smallest detent torque. To allow for a relevant comparison among topologies, the current density was slightly increased in the models with a higher number of poles, which produced almost the same Joule losses in the motors, limited by technical specification at 9 W.

The dots on the graphics below, Fig. 14 - Fig. 18, are points of computation (there is no interpolation in between). To achieve these characteristics a rotational step of 0.03° was used for computing the holding torque, and a step with a value between 0.0075° and 0.015° to determine the detent torque. Due to the characteristics' symmetry, only half of the period was computed for each curve. Despite simplifications and the reduced calculation domains, each characteristic required hours of computation [9].

The HSM with the lowest detent torque was the motor with 48 poles, Fig. 18. However, further optimization of the other topologies could lead to a reduction of the existing detent torque values. As a rule, decreasing the detent torque attracts a reduction of the holding torque too. Also, motors with permanent magnets having a cross-section closer to a square seemed to produce a lower detent torque.

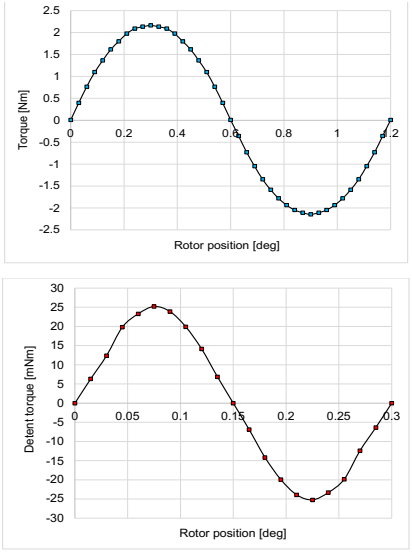

Fig. 14 – The 16-pole HSM mechanical characteristics: holding torque (above), detent torque (below).

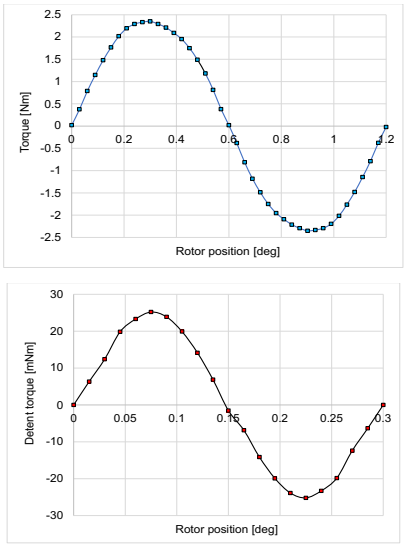

Fig. 15 – The 24-pole HSM mechanical characteristics: holding torque (above), detent torque (below).

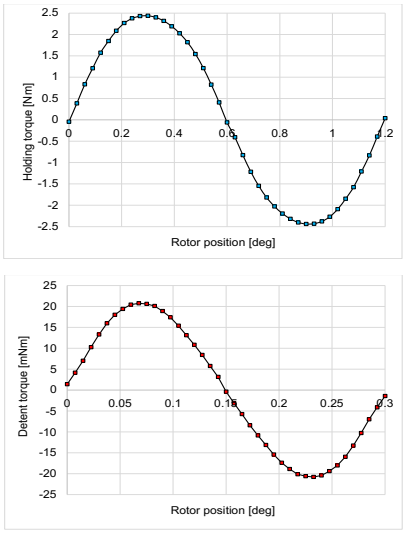

Fig. 16 – The 32-pole HSM mechanical characteristics: holding torque (above), detent torque (below).

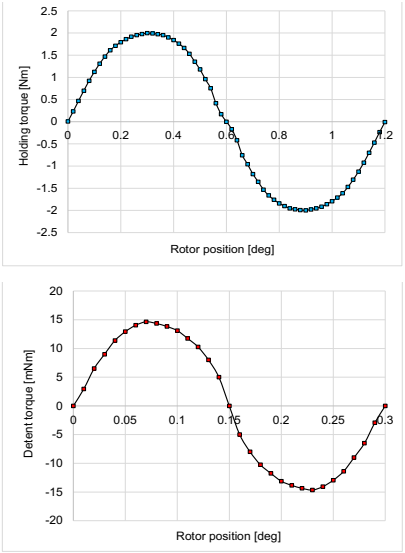

Fig. 17 – The 40-pole HSM mechanical characteristics: holding torque (above), detent torque (below).

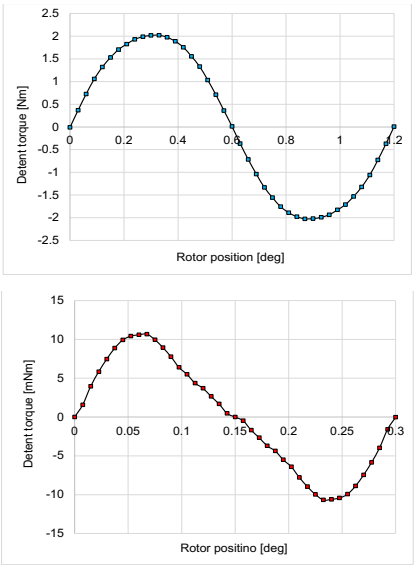

Fig. 18 – The 48-pole HSM mechanical characteristics: holding torque (above), detent torque (below).

In *Table 2* are listed the main HSM specifications. A higher number of stator poles allows for increasing the motor torque density up to a point. Increasing the number of poles may have the opposite result, but the HSMs with a higher number of poles produce a reduced detent torque.

Table 2

Main technical specifications of the studied HSM topologies

	Motor version	16-pole	24-pole	32-pole	40-pole	48-pole
Rotor length	mm	14	18	22	22	24
Total length	mm	31	31	31	29	29
Inner diameter	mm	121	125	125	126	125
Outer diameter	mm	157	157	157	157	157
Airgap length	mm	0.25	0.25	0.25	0.25	0.25
Rotor weight	g	350	460	491	525	557
Stator weight	g	390	420	560	495	610
Rotor inertia	g·m^2	1.56	2.3	2.5	2.3	2.7
Current density	A/mm^2	1.44	1.46	1.5	1.73	1.73
Holding torque	Nm	2.16	2.34	2.45	1.9	2.01
Detent torque	mNm	25	25	20	14	11

At the same time, the motors with a higher number of poles have shorter end windings, and thus current density can be slightly increased to produce the same Joule losses. They can also be made longer, but then they become heavier. In contrast, motors with fewer poles have wider slot openings and larger stator yokes, being technologically easier to manufacture than the higher pole number motors.

4. CONCLUSIONS

Increasing the number of stator poles makes possible the reduction of the end windings and the extension of the lamination stack when the motor axial length is imposed. That can be an advantage when higher torque densities are required. On the other hand, a longer axial length means an increased rotor weight and a higher moment of inertia. This paper presents the practicality of changing the number of stator poles for a bi-phase hybrid stepper with 300 rotor teeth with reduced dimensions and a small difference between the motor's outer and inner diameter.

The bi-phase stepper motors must have a multiple of four stator poles with their teeth shifted against the rotor teeth at 0, 90, 180, and 270 electric degrees, respectively. To achieve the teeth alignment for the 24-pole and 40-pole HSM topologies, a simple but original method was proposed in this paper, consisting of shifting two out of every four poles with a predetermined tiny angle.

The results confirm that choosing a larger number of stator poles assists in a better distribution of the winding and more efficient use of the stator space. However, when the number of poles is too high, the stator yoke and the pole width become too small, which makes motor manufacturing difficult. Therefore, the topology with 24 poles was chosen for production among the five presented technologies. The 32-pole stepper, while having a slightly better performance (higher holding torque and slightly reduced detent torque) than the 24-pole topology, requires more labor and has a very thin stator yoke, which can cause mechanical deformation.

Computing the stepper holding and the detent torque characteristics for each constructive variant was time-consuming, each characteristic requiring several hours of computation. A much more refined/dense discretization mesh and a finer rotor moving step were used to compute the detent torque. Compared to hybrid 2D-analytical models used for designing HSM proposed in [4,6,16], the models and results presented in this paper are more accurate. They can provide a good practical insight into modeling such motors. According to the authors' research, the 300 teeth stepper (with 0.3° full step) is very rare, and even fewer were thoroughly modeled. To avoid the complexity of such a study and the computation effort, most steppers are produced in series of the same frame (usually NEMA 8,11,14,17,23 and 34), by extending the rotor using a multi-stack construction [16]. A complete and accurate analytical computation of the hybrid stepper is practically impossible to achieve, as this cannot account accurately for the magnetic flux leakage and fringing [18].

This research will be completed later with relevant experimental results once the 24-pole stepper is executed.

Received on 2 February 2023

REFERENCES

1. P. Li, H. Lu, J.V.V. Athani, *Stepper Motors: Fundamentals, Applications and Design*, New Age International (1997).
2. C. Stuebig, B. Ponick, *Comparison of calculation methods for hybrid stepping motors*, in IEEE Transactions on Industry Applications, **48**, *6*, pp. 2182–2189 (Nov.-Dec. 2012).
3. M. Onsal, Y. Demir, M. Aydin, M.K. Guven, *Impact of airgap on the performance of 3-phase permanent magnet hybrid stepper motor,* IECON 2021 – 47th Annual Conference of the IEEE Industrial Electronics Society, Toronto, ON, Canada, pp. 1–5 (2021).
4. Ki-Bong Jang, Seong-Yeop Lim, Tae-Bin Lim, Chang-Sung Jin, Yun-Hyeon Cho, Young-Tae Kim, and Ju Lee, Member, IEEE, *2-D FE analysis of hybrid stepping motor using a virtual magnetic barrier*, IEEE Transactions on Magnetics, **39**, *5* (2003).
5. E.C.T. So, S.J. Yang, *The effect of tooth shape on radial forces in step motors*, IEEE Transactions on Magnetics, **29**, *6*, pp. 2413–2415, (1993).
6. R.P. Praveen, M.H. Ravichandran, V.T.S. Achari, V.P. Jagathy Raj, G. Madhu, G.R. Bindu, *Design and finite element analysis of hybrid stepper motor for spacecraft applications*, IEEE International Electric Machines and Drives Conference, pp. 1051–1057 (2009).
7. I. Ionică, M. Modreanu, A. Morega, C. Boboc, *Design and modeling of a hybrid stepper motor*, 2017 10th International Symposium on Advanced Topics in Electrical Engineering (ATEE), Bucharest, Romania, pp. 192–195 (2017).
8. I. Ionică, M. Modreanu, A. Morega, C. Boboc, *Numerical analysis of a hybrid stepper motor for the electromagnetic torque calculation*, 2019 11th International Symposium on Advanced Topics in Electrical Engineering (ATEE), Bucharest (2019).
9. O. Craiu, T.I. Ichim, L. M. Melcescu, L. Popescu, *Optimization of a High Torque Density Small Hybrid Stepper using 3D FEM Model*, 2022 International Symposium on Power Electronics, Electrical Drives, Automation and Motion (SPEEDAM), pp. 610–615 (2022).
10. I. Ionică, M. Modreanu, A. Morega, C. Boboc, *Geometry Influence on the Electromagnetic Torque Calculation of a Stepper Motor*, 2021 12th International Symposium on Advanced Topics in Electrical Engineering (ATEE), pp. 1–7 (2021).
11. K.R. Rajagopal, B. Sing, B.P. Singh, *Optimal tooth-geometry for specific performance requirements of a hybrid stepper motor*, in IEEE Transactions on Magnetics, **39**, *5*, pp. 3010–3012, Sept. 2003.
12. ***AC/DC Module User's Guide©, 1998–2020, COMSOL Multiphysics, Version: COMSOL 5.6.
13. O. Craiu, T.-I. Ichim, L.C. Popescu, *3D fem model of a hybrid stepper using scalar-vector potential formulations*, 2023 13th International Symposium on Advanced Topics in Electrical Engineering (ATEE), Bucharest, Romania, pp. 1–5 (2023).
14. A. Arkkio, Analysis of Induction Motors Based on the Numerical Solution of the Magnetic Field and Circuit Equations, PhD Thesis, Helsinki (1987).
15. P. Li, H. Lu, J. Shen, *Analysis method of dynamic torque-frequency characteristic of hybrid stepping motors*, 2017 Twelfth International Conference on Ecological Vehicles and Renewable Energies (EVER), pp. 1–6 (2017).
16. K.R. Rajagopal, M. Krishnaswamy, B. Sing, B.P. Singh, *An improved high-resolution hybrid stepper motor for solar-array drive of Indian remote-sensing satellite*, in IEEE Transactions on Industry Applications, **33**, *4*, pp. 906–913 (1997).
17. *** https://www.nema.org/standards/view/motors-and-generators
18. M. Bjekić, A, Milovanovic, B. Koprivica *Prediction of pull-in and pull-out torque characteristics of the permanent magnet step motor*, Rev. Roum. Sci. Techn. – Électrotechn. Et Énerg.,**60**, *1*, pp. 29–38 (2015).